Canadian Mineralogist
Vol. 16, pp. 625-640 (1978)

THE TANCO PEGMATITE AT BERNIC LAKE, MANITOBA. XI. NATIVE ELEMENTS, ALLOYS, SULFIDES AND SULFOSALTS*

P. ČERNÝ
Department of Earth Sciences, University of Manitoba, Winnipeg, Manitoba R3T 2N2

D. C. HARRIS
Canada Centre for Mineral and Energy Technology, 555 Booth Street, Ottawa, Ontario K1A 0G1

Abstract

Native elements, alloys, sulfides and sulfosalts occur within the latest zones of the Tanco pegmatite. The spodumene-(petalite-) rich zones (4) and (5) contain diffuse patches of antimonian bismuth, bismuthian antimony, bismuthian stibarsen, arsenic, galena, sphalerite, chalcopyrite, tetrahedrite and dyscrasite; scattered grains of sphalerite and molybdenite occur separately. The tantalum ore bodies produced by albitization (3) of the central intermediate zone (6) contain arsenopyrite, pyrrhotite and chalcopyrite in the biotite + tourmaline-rich contacts of amphibolite xenoliths, sphalerite as isolated grains, and Tl-enriched botryoidal pyrite + marcasite in open vugs. Cavity- and fissure-filling assemblages in this zone (6) consist of early pyrrhotite, cubanite, sphalerite, hawleyite, chalcopyrite, bismuth and later stannite, kesterite, and černýite closely associated with cassiterite. All these minerals were subsequently replaced and/or cemented by galena, gustavite, gladite–pekoite, cosalite, tetrahedrite, freibergite, bournonite, pyrargyrite, miargyrite and bismuthian antimony. In both parent zones, late minerals of the complex assemblages occur in extremely fine-grained aggregates. Some of these resulted from quench-induced mass precipitation, and others suggest quench-arrested incomplete replacement reactions. Rapid crystallization and quenching of non-equilibrium associations are responsible for the variety and broad extent of substitutions observed in most species, and for the generation and preservation of metastable phases. Crystallization of the complex sulfide assemblages probably proceeded at about 200–150°C, with $f(S_2)$ as low as 10^{-20} to 10^{-22} atm.

Sommaire

On trouve les éléments natifs, alliages, sulfures et sulfosels dans les zones les plus tardives de la pegmatite Tanco. Les zones (4) et (5), riches en spodumène (pétalite), contiennent des amas diffus de bismuth antimonique, antimoine et stibarsène bismuthiques, arsenic, galène, sphalérite, chalcopyrite, tétraédrite et dyscrasite, et, séparément, des grains éparpillés de sphalérite et de molybdénite. Les gîtes de tantale qui résultent de l'albitisation (3) de la zone centrale intermédiaire (6) contiennent l'assemblage arsénopyrite–pyrrhotine–chalcopyrite dans les contacts riches en biotite et tourmaline autour de xénolithes d'amphibolite; de la sphalérite en grains isolés, et de la pyrite botryoïde riche en Tl avec marcasite dans les cavités non-remplies. Dans cette zone (6), les assemblages qui remplissent les cavités et les fissures consistent en minéraux précoces (pyrrhotine, cubanite, sphalérite, hawleyite, chalcopyrite, bismuth) et en minéraux plus tardifs (stannite, kesterite et černýite) étroitement associés à la cassitérite. Tous ces minéraux ont été remplacés ou cimentés par les espèces suivantes: galène, gustavite, gladite–pékoïte, cosalite, tétraédrite, freibergite, bournonite, pyrargyrite, miargyrite et antimoine bismuthique. Dans les deux zones mères, les minéraux tardifs des assemblages complexes se trouvent en agrégats à grain extrêmement fin. Certains de ceux-ci résultent d'une précipitation massive provoquée par une trempe; d'autres font supposer des réactions de remplacement interrompues par la trempe. La cristallisation rapide et la trempe d'associations en déséquilibre sont à l'origine de la variété et l'étendue des substitutions observées dans la majorité des espèces, ainsi que de la formation et de la préservation de phases métastables. La cristallisation des assemblages complexes de sulfures a probablement eu lieu entre 200 et 150°C, à basse fugacité de soufre (10^{-20} à 10^{-22} atm).

(Traduit par la Rédaction)

Introduction

Although the frequency and abundance of sulfide minerals in granitic pegmatites is quantitatively insignificant, sulfide assemblages deserve attention because they form an inherent part of the geochemistry of pegmatites and aid in their petrogenetic classification. Bulk compositions of some sulfide assemblages tend to be exotic, produced by crystallization in complex pegmatitic systems; they deviate considerably

*Centre for Precambrian Studies Publication No. 27.

from those of more ordinary hydrothermal sulfide parageneses. Consequently, minerals with a complex crystal chemistry may have an unusual range of compositions, leading, in extreme cases, to unique mineral species that do not occur in other geological environments.

Particularly remarkable in this latter aspect is the Tanco pegmatite at Bernic Lake, southeastern Manitoba. This giant deposit of Li,Rb, Cs,Ta,Be and of several industrial minerals belongs to the most complex pegmatites in the world (R. A. Crouse *et al.*, in prep.). The ratios K/Rb, Rb/Cs, Nb/Ta, Fe/Mn and Zr/Hf in constituent minerals mark this pegmatite as a product of extremely advanced geochemical fractionation. Investigations of sulfide minerals from this deposit have already led to the characterization of gustavite (Harris & Chen 1975) and to the understanding of the aikinite–bismuthinite series (Harris & Chen 1976); the pegmatite has also yielded a new mineral species (černýite: Kissin *et al.* 1978, Szymański 1978). Native elements, alloys, sulfides and sulfosalts identified to date (Table 1) exceed the number of silicate phases constituting the bulk of the pegmatite. Mineralogy and paragenetic relations of this sulfide assemblage are the subject of the present paper.

Sampling and Experimental Methods

Owing to the scarcity of sulfides in the Tanco pegmatite, all specimens found since 1969 were saved and subjected to routine optical examination. Sixty-eight samples were selected for detailed study and several dozen others were briefly examined to improve the statistical basis of certain observations.

Because of the fine grain-size of most aggregates and the optical similarity of most sulfosalts encountered, the MAC 400 electron microprobe was the main tool of investigation. Pure metals and synthetic compounds were used as standards throughout the study, and the microprobe data were corrected by using the EMPADR VII computer program of Rucklidge & Gasparrini (1969). An X-ray powder diffractometer was used initially for mineral identification in complex mixtures and for selected cell-dimension refinements. Most refinements, however, were based on Debye-Scherrer, Gandolfi and precession films.

Occurrences in the Pegmatite

The Tanco pegmatite is a subhorizontal lenticular body with complex internal structure, consisting of 9 primary zones and replacement units. Detailed description and illustration of the zoning pattern are given by Crouse & Černý (1972), Černý & Simpson (1978) and Crouse *et al.* (in prep.). The sulfides and related minerals are restricted to the central zones of the Tanco deposit. Most of the specimens were obtained from the central intermediate zone (6) that has been penetrated by a saccharoidal albite unit (3); sulfides are much less common in the lower and upper intermediate zones, numbered (4) and (5), respectively.

The central intermediate zone (6) consists mainly of coarse grey microcline perthite and quartz, with minor primary albite. The zone is veined and replaced by albite and fine-grained greenish muscovite of the metasomatic unit (3). These minerals appear in various textural patterns, and they have abundant Ta, Sn, Zr–Hf and Be mineralization. Zones (4) and (5), which more or less envelop the central intermediate zone (6), consist mainly of giant-sized petalite (mostly converted to spodumene

TABLE 1. SULFIDE MINERAL ASSEMBLAGES IN THE TANCO PEGMATITE

Mode of occurrence	Assemblage # in zones (4) and (5)		Assemblage # in zones (3) and (6)		
Contacts with amphibolite xenoliths	-	-	(6,3A)	arsenopyrite pyrrhotite chalcopyrite	
Dispersed isolated grains	(4,5A) (4,5B)	sphalerite molybdenite	(6,3B)	sphalerite	
Cavity- and fissure-filling aggregates	(4,5C)	bismuthian antimony antimonian bismuth bismuthian stibarsen arsenic galena sphalerite chalcopyrite tetrahedrite dyscrasite	(6,3C)	bismuth bismuthian antimony pyrrhotite sphalerite hawleyite pyrite arsenopyrite cubanite chalcopyrite galena	stannite kesterite černýite cosalite gustavite gladite-pekoite tetrahedrite freibergite bournonite pyrargyrite miargyrite
Miarolitic cavities	-	-	(6,3D)	pyrite marcasite	

+ quartz), quartz, amblygonite–montebrasite, and microcline perthite. Zone (4) occurs mainly in the lower part of the pegmatite and is enriched in cleavelandite and micas whereas zone (5) occupies the hanging-wall side; the size of its mineral constituents is much larger, and its albite and mica contents are rather low.

Seven sulfide assemblages have been recognized in the above zones (Table 1). Individual mineral assemblages are designated by letters without genetic meaning, designed to simplify references in the text below.

Assemblages in zones (4) and (5)

Sphalerite occurs as disseminated grains and aggregates mainly on and within spodumene + quartz pseudomorphs after petalite. Individual crystals containing twin lamellae reach 3 cm in maximum dimension, and medium-grained clusters measure as much as 8 cm across. No other minerals are associated with this type of sphalerite, designated (4,5A).

Most of the molybdenite is also isolated from other sulfides. Single flakes or small pods, designated (4,5B), are found mostly in quartz, and occasionally in the spodumene–quartz intergrowths.

Assemblage (4,5C) consists of native antimony, bismuth, arsenic, stibarsen, dyscrasite, galena, chalcopyrite, sphalerite and tetrahedrite. This mixture forms dendritic patches in spodumene + quartz pseudomorphs, surrounds the spodumene fibres and has apparently corroded quartz. Rare, more massive sulfide blebs fill fissures in quartz.

Assemblages in zone (6) associated with albitization (3)

Assemblage (6,3A), arsenopyrite + pyrrhotite + chalcopyrite, typically occurs in reaction rims that separate the pegmatite from xenoliths of amphibolite wallrock. The most abundant reaction products are tourmaline adjacent to amphibolite, and biotite adjacent to the pegmatite side of the contact. Holmquistite occasionally is present inside the amphibolite inclusions, and triphylite or beryl may occur on the pegmatite side of the biotite band. Arsenopyrite is largely confined to the tourmaline zone but some grains also occur inside the pegmatite. Pyrrhotite and chalcopyrite are located along the biotite–pegmatite boundary, commonly associated with triphylite.

Sphalerite designated (6,3B) occurs as isolated irregular grains disseminated in quartz, microcline perthite and muscovite.

The most complex assemblage (6,3C) is found as cavity- and fissure-fillings in the silicate matrix. A total of 21 mineral species were identified (Table 1). Except for gladite–pekoite intergrowths in columnar "crystals" up to 4 cm long, and occasional 5 to 8 mm patches of tetrahedrite, the sulfides typically have an average grain size of about 10 μm. Pyrrhotite, bismuth, chalcopyrite, gladite–pekoite and tetrahedrite are the most common and abundant constituents of the aggregates; traces of pyrite have been found only once.

Botryoidal pyrite + marcasite (assemblage 6,3D) occur mostly in open cavities lined with quartz and microcline crystals, associated with cookeite, apatite and calcite.

Mineral Descriptions

Native elements and alloys

Native bismuth, antimony, arsenic, stibarsen and dyscrasite occur in the Tanco pegmatite. Assemblage (4,5C) consists of all five minerals, but only bismuth and bismuthian antimony were identified from (6,3C).

Bismuth in assemblage (4,5C) occurs either as fine-grained emulsion-like intergrowths with galena or as irregular granular aggregates with antimony, arsenic and stibarsen (Fig. 1). Concentric overgrowths displaying different crys-

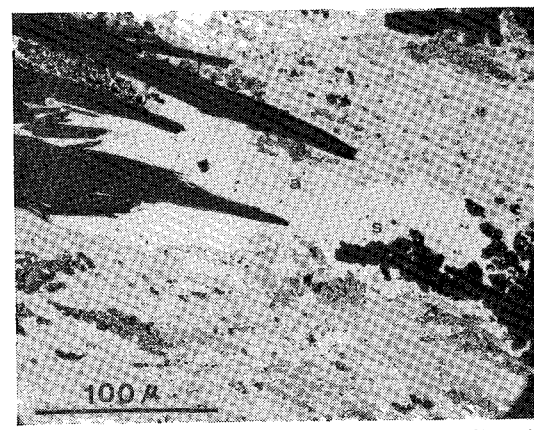

FIG. 1 Concentric aggregate of bismuth (small grain in centre) overgrown by arsenic (dark grey, a) and stibarsen (light grey, s) flanked by bismuth and antimony to the right, and by bismuth and dyscrasite to the left (all white). Guttate bismuth in galena constitutes the adjacent areas between fibrous spodumene and deeply corroded relics of quartz. Assemblage (4,5C), polished section in oil immersion, polarized light.

TABLE 2. ELECTRON MICROPROBE ANALYSES OF NATIVE ELEMENTS AND ALLOYS

Assemblage	Arsenic	Stibarsen	Antimony	Bismuth							Dyscrasite
		(4,5C)		(4,5C)				(6,3C)			(6,3C)
Anal.#	S-50-1	S-50-2	S-50-3	S-51-1	S-50-I	S-50-II*	S-51-2*	S-27	S-2-1	S-2-2*	S-50
As	99.4	40.3	1.5	- **	-	-	-	-**	-	-	.3
Sb	1.4	57.4	84.7	2.6	11.1	13.8	2.0	-	1.5	1.9	23.7
Bi	1.2 ***	4.5	13.4	97.7	89.8	86.2	98.0	100.1	98.4	98.1	.8
Ag	n.d.	n.d.	n.d.	n.d.	n.d.	n.d.	n.d.	n.d.	n.d.	n.d.	77.0
	102.0	102.2	99.6	100.3	100.9	100.0	100.0	100.1	99.9	100.0	101.8

S-50-1 $As_{.987}Sb_{.008}Bi_{.004}$
S-50-2 $Sb_{.458}As_{.522}Bi_{.020}$
S-50-3 $Sb_{.892}Bi_{.082}As_{.026}$

S-51-1 $Bi_{.957}Sb_{.043}$
S-50-I $Bi_{.825}Sb_{.175}$
S-50-II* $Bi_{.785}Sb_{.215}$
S-51-2* $Bi_{.967}Sb_{.033}$

S-27 $Bi_{1.00}$
S-2-1 $Bi_{.975}Sb_{.025}$
S-2-2* $Bi_{.968}Sb_{.032}$
S-50 $Ag_{3.000}(Sb_{.819}As_{.017}Bi_{.017})\ \Sigma.853$

Analysts: bismuth - G. Laflamme, others - D.C. Harris; *Bi calculated to 100.0%; **not detected; ***not determined.

tallization sequences seem to be characteristic; exsolution phenomena, a feature typical of other pegmatitic occurrences of stibarsen (Quensel *et al.* 1937, Wretblad 1941, Černý & Harris 1973) have not been observed. The bismuth is rich in Sb (Table 2); *antimony* is Bi-bearing, with some As, and in this respect very similar to bismuthian antimony from the Viitaniemi pegmatite (Volborth 1960). In contrast, *arsenic* is rather pure, and the Bi content of stibarsen is negligible. However, *stibarsen* (ideally, SbAs) deviates significantly from this composition (*cf.*, Černý & Harris 1973, Table 2).

Dyscrasite occurs closely associated with the above four minerals (Fig. 1). Microprobe analysis (Table 2) gives a formula extremely close to Ag_7Sb_2. In relation to the dyscrasite stability field as defined by Somanchi (1966) and Keighin & Honea (1969) and modified by Petruk *et al.* (1971a), this composition falls just inside the Ag-rich boundary, and somewhat farther into the field when the Sb content is combined with Bi and As.

In assemblage (6,3C), *bismuth* occurs intimately intergrown with pyrrhotite, sphalerite and chalcopyrite. In places, bismuth and chalcopyrite seem to have formed later than the other two minerals. Bismuth in small patches associated with late sulfosalts contains variable Sb, approaching bismuthian antimony; otherwise, the Sb content of bismuth is low.

Sulfides

The most common sulfide minerals are sphalerite, pyrite, marcasite, pyrrhotite, arsenopyrite, molybdenite, chalcopyrite and galena, with minor cubanite and hawleyite.

Sphalerite, the most widespread sulfide species at Tanco, is fairly abundant as randomly dispersed grains and small clusters in zones (4), (5) and (6); it is usually not accompanied by other sulfides; in a single specimen from the assemblage (6,3B) it occurs with minor pyrite and galena. A pale sulfur-yellow color is characteristic of sphalerite (4,5A), and yellow to medium brown is typical of (6,3B). In zone (5), sphalerite commonly occurs in small pods of rhodochrosite, lithiophilite, quartz and Ta-oxide minerals.

In contrast to its abundance in disseminated form, sphalerite is subordinate in the most diversified assemblage, (6,3C). Here it occurs as microscopic anhedral grains associated with native bismuth, pyrrhotite and chalcopyrite.

The different paragenetic types of sphalerites are indicated by their compositions (Table 3). Sphalerite (6,3C) is exceptionally rich in Cd and distinctly enriched in Fe, whereas sphalerites (4,5A) and (6,3B) have lower Cd and Fe contents. Unit-cell dimensions, determined only for the coarse-grained varieties of sphalerite, are in good agreement with those calculated from Skinner's (1961) equations.

Pyrite and *marcasite* are virtually restricted to assemblage (6,3D); they form fine-grained botryoidal crusts on quartz, cookeite, apatite and calcite in open vugs of the central intermediate zone. Pyrite is the more abundant and common of the two. The only other occurrence of pyrite, besides that quoted in the description of sphalerite, is known from a single sulfide aggregate in assemblage (6,3C).

Electron microprobe analysis of pyrite and marcasite (6,3D) did not reveal any elements other than Fe and S, and unit-cell dimensions determined for five samples of pyrite from different cavities fall within the range quoted for pure cubic FeS_2. Mr. C. Dallaire (Laboratoire de Géochimie Analytique, Ecole Polytechnique, Montréal) detected considerable Tl in three specimens of pyrite: 121, 192, and 820 ppm.

TABLE 3. ELECTRON MICROPROBE ANALYSES OF SPHALERITE AND HAWLEYITE

	Sphalerite									Hawleyite			
Assemblage	(6,3C)			(6,3B)		(4,5A)				(6,3C)			
Anal.#	A-16A	S-3-1	S-3-2	S-58	S-66	S-24	S-25	S-30	S-44	S-21	S-22	S-2-3	S-3
In	-*	n.d.**	n.d.	n.d.	n.d.	.05	.03	.03	n.d.	n.d.	n.d.	n.d.	n.d.
Mn	-	n.d.	n.d.	.03	-	.05	.02	.03	.1	n.d.	n.d.	n.d.	n.d.
Fe	6.8	5.4	5.6	.8	1.6	.2	.20	.3	.6	-	-	-	1.7
Cd	6.9	11.9	17.6	1.4	1.4	1.7	1.6	1.8	1.7	71.5	72.4	70.4	70.5
Zn	52.5	48.3	43.7	64.4	64.6	65.4	66.0	65.2	64.5	5.3	4.4	6.4	6.2
S	31.7	31.5	30.9	33.0	32.3	33.0	32.4	32.9	32.5	22.8	22.0	22.1	22.6
	97.9	97.1	97.8	99.63	99.9	100.40	100.25	100.26	99.4	99.6	98.8	98.9	101.0
a (Å) meas.***				5.4154(7)	5.4155(6)	5.4157(8)	5.4154(6)	5.4162(7)	5.4166(5)				
a (Å) calc.				5.4155	5.4155	5.4159	5.4153	5.4165	5.4165				

S-16A $(Zn_{.812}Fe_{.123}Cd_{.062})\ \Sigma.996S_{1.000}$
S-3-1 $(Zn_{.752}Fe_{.098}Cd_{.108})\ \Sigma.958S_{1.000}$
S-3-2 $(Zn_{.694}Fe_{.104}Cd_{.162})\ \Sigma.960S_{1.000}$
S-58 $(Zn_{.957}Fe_{.014}Cd_{.012})\ \Sigma.983S_{1.000}$
S-66 $(Zn_{.981}Fe_{.028}Cd_{.012})\ \Sigma1.021S_{1.000}$
S-24 $(Zn_{.972}Cd_{.015}Fe_{.003})\ \Sigma.990S_{1.000}$
S-25 $(Zn_{.999}Cd_{.014}Fe_{.003})\ \Sigma1.016S_{1.000}$
S-30 $(Zn_{.972}Cd_{.016}Fe_{.005}Mn_{.001})\ \Sigma.994S_{1.000}$
S-44 $(Zn_{.974}Cd_{.015}Fe_{.011}Mn_{.002})\ \Sigma1.002S_{1.000}$
S-2-1 $(Cd_{.894}Zn_{.114})\ \Sigma1.008S_{1.000}$
S-2-2 $(Cd_{.939}Zn_{.098})\ \Sigma1.037S_{1.000}$
S-2-3 $(Cd_{.909}Zn_{.142})\ \Sigma1.041S_{1.000}$
S-3 $(Cd_{.890}Zn_{.134}Fe_{.043})\ \Sigma1.007S_{1.000}$

Analysts: Sphalerites S-24,25,30 - D.R. Owens; others - D.C. Harris
*not detected, **not determined, ***using Skinner's (1961) equation

Monoclinic pyrrhotite occurs as scattered grains within and close to the biotite seams of assemblage (6,3A), and as one of the earliest phases in the fine-grained sulfide pods (6,3C). Monoclinic pyrrhotite has never been found associated with hexagonal pyrrhotite or pyrite. This indicates that it originated by direct crystallization rather than by reequilibration of pre-existing Fe-sulfide minerals. Electron microprobe analyses of pyrrhotite from sample *S–11A* gave 60.9 wt. % Fe and 39.7 wt. % S (total = 100.6) yielding the formula $Fe_{7.04}S_{8.00}$. This stoichiometry is very close to the "ideal" composition of monoclinic pyrrhotite (Kissin 1974; Craig & Scott 1974).

Arsenopyrite forms typical prismatic crystals in its two assemblages. In (6,3A), subhedral crystals usually less than 2 mm long are dispersed in brownish-black tourmaline or, rarely, biotite. In albite and quartz adjacent to the reaction rims of this assemblage, arsenopyrite individuals reach 2 cm in length. In (6,3C), arsenopyrite was found only in a single specimen. It is euhedral, somewhat fractured and cemented by later sulfides and native bismuth.

Four analyses quoted in Table 4 represent samples from the tourmaline reaction bands (A,B), from albite-rich pegmatite near these bands (*S*-10), and from the (6, 3C) assemblage (*S*-3). All four analyses suggest slight excess of Fe, but within the standard error calculated for the highly accurate analyses of Kretschmar & Scott (1976). More significantly, all specimens are distinctly As-rich and deficient in S. The arsenic contents, 34.5–35.3 at. % as determined by microprobe analyses, are somewhat higher than those inferred by the X-ray method of Kretschmar & Scott (1976), 34.1–35.0 at. %. This difference may be due to the choice of microprobe standards or inhomogeneity of the crystals.

Molybdenite occurs as scattered isolated flakes in the assemblage (4,5B). Patches of native elements, chalcopyrite and sulfosalts containing euhedral flakes of molybdenite are exceptional. X-ray powder diffraction data of 19 molybdenite samples gave only the $2H_1$ polytype. Although the possible compositional and genetic differences between the $2H_1$ and $3R$ polytypes are still not unequivocal, the exclusive occurrence of $2H_1$ in the Tanco pegmatite fits the previously defined patterns: generally late, low-

TABLE 4. ELECTRON MICROPROBE ANALYSES OF ARSENOPYRITE

Assemblage	(6,3A)			(6,3C)
Anal.#	A	B	S-10	S-3
Fe	34.2	34.3	34.6*	34.4
Co	.2	.1	n.d.	n.d.
As	48.5	47.8	47.4	49.0
Sb	.05	.04	n.d.	n.d.
S	18.0	18.8	18.7	18.0
	100.95	101.04	100.7	101.4
a (Å)	5.797(3)	5.783(4)	5.789(3)	5.802(2)
b (Å)	5.706(1)	5.698(2)	5.696(1)	5.708(1)
c (Å)	5.789(2)	5.786(2)	5.784(2)	5.788(2)
β	112°36 (4)'	112°35 (4)'	112°35 (3)'	112°42 (3)'
V (Å³)	176.78 (4)	176.04 (6)	176.10 (4)	176.83 (3)

A $(Fe_{1.007}Co_{.005})\ \Sigma1.012(As_{1.065}S_{.924}Sb_{.001})\ \Sigma1.990$
B $(Fe_{1.002}Co_{.003})\ \Sigma1.005(As_{1.041}S_{.956}Sb_{.001})\ \Sigma1.998$
S-10 $Fe_{1.013}(As_{1.034}S_{.953})\ \Sigma1.988$
S-3 $Fe_{1.009}(As_{1.071}S_{.919})\ \Sigma1.990$

Analysts: A,B - D.R. Owens, S-10,3 - D.C. Harris;
*not determined.

temperature origin of the S-deficient, Re-enriched $3R$ polytype in copper-rich environments, and relatively high-temperature crystallization of metal-deficient, Re-poor $2H_1$ polytype in pegmatites, greisens and other Cu-poor parageneses (Khurshudyan 1967, Boyle 1969, Clark 1970, 1971; Frondel & Wickman 1970, Znamenskiy *et al.* 1970, Angelelli *et al.* 1971, Ayres 1974). Other factors such as rate of crystallization may also affect polytypism (Yang *et al.* 1975).

Chalcopyrite occurs predominantly in the assemblage (6,3A), although small amounts are dispersed in the biotite seams as single grains or with pyrrhotite. In (6,3C) chalcopyrite has two modes of occurrence. The first is with the earlier pyrrhotite, sphalerite, bismuth and stannite-group minerals, in the marginal parts of the sulfide aggregates; the second occurrence, with later sulfosalts, forms linings of gangue-filled microscopic vugs. Two microprobe analyses yielded formulas identical with the formula of chalcopyrite, within the limits of analytical error.

Galena occurs in two assemblages. In (4,5C), it hosts very fine-grained emulsion-like aggregates of bismuth (Fig. 1). In (6,3C), galena accompanies chalcopyrite and native bismuth associated with early pyrrhotite, and also is common as relict intergrowths with the late sulfosalts. Microprobe analyses of galena revealed only Pb and S.

Cubanite forms anhedral inclusions in pyrrhotite, and is also associated with cosalite. A microprobe analysis indicates the ideal formula for this species. Only a single X-ray powder pattern of sulfide mixtures permitted unequivocal identification of the Tanco cubanite as the low-temperature orthorhombic polymorph.

Hawleyite occurs as minute grains associated with native bismuth, pyrrhotite and chalcopyrite in assemblage (6,3C). Although hawleyite was never found in contact or closely associated with sphalerite, both occur in the same sulfide nodules. Its composition (Table 3) is fairly rich in Zn (10–14 mol. % ZnS) but has lower Fe than sphalerite from the same assemblage. Owing to its minute grain-size, hawleyite could not be confirmed by X-ray diffraction, but its composition and isotropic optical properties justify the identification.

Sulfosalts

Stannite, černýite and *kesterite* are restricted to the assemblage (6,3C). They are closely associated with cassiterite, which they commonly corrode and replace (Fig. 2). Stannite is the most abundant, černýite very subordinate, and kesterite rare. The three minerals form irregular patchy intergrowths and occasional concentrically zoned grains (Fig. 3); no exsolution textures were observed.

Compositional variations in this mineral group are extensive (Table 5, Fig. 4) but no significant deviations from the general formula A_2BCS_4 were encountered. Most of the stannites are low in both Zn and Cd, but some analyses show up to 40 mol. % of the Zn component. A positive

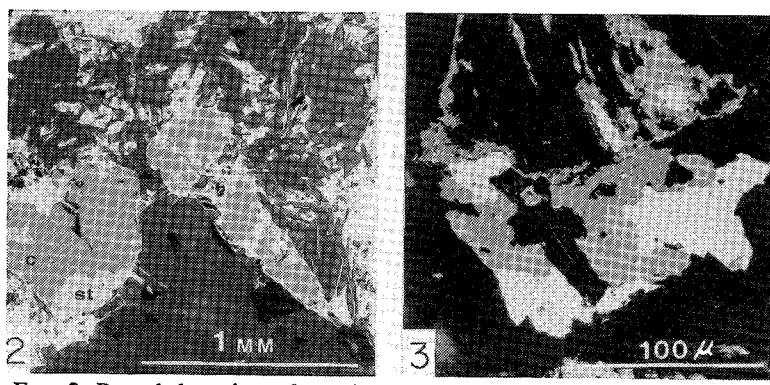

FIG. 2 Rounded grains of cassiterite (medium grey, c) corroded and partly replaced by stannite (light grey, st). Muscovite adjacent to the cassiterite is penetrated by fine-grained bismuth, chalcopyrite, pyrrhotite and sulfosalts. Assemblage (6,3C), polished section, polarized light.

FIG. 3 Cassiterite (black) corroded and replaced by stannite and černýite (darker and lighter grey, respectively). Chalcopyrite and bismuth constitute the white areas. Assemblage (6,3C), polished section in oil immersion, polarized light.

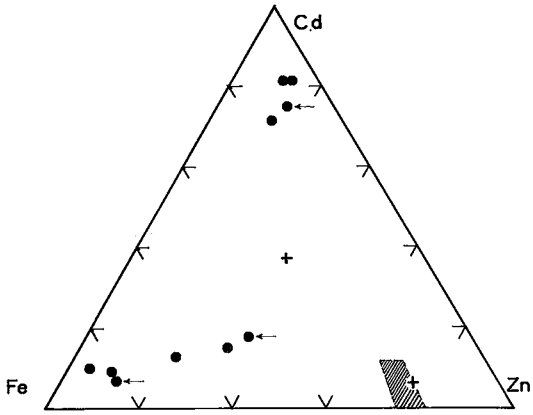

FIG. 4 Composition of stannite, černýite and kesterite in terms of the (Fe,Cd,Zn)-site population (at.%). Tanco compositions are marked by dots (and by a shaded area for the probable composition of kesterite). Compositions from the Hugo pegmatite (crosses) and the dots with an arrow are from Kissin *et al.* (1978).

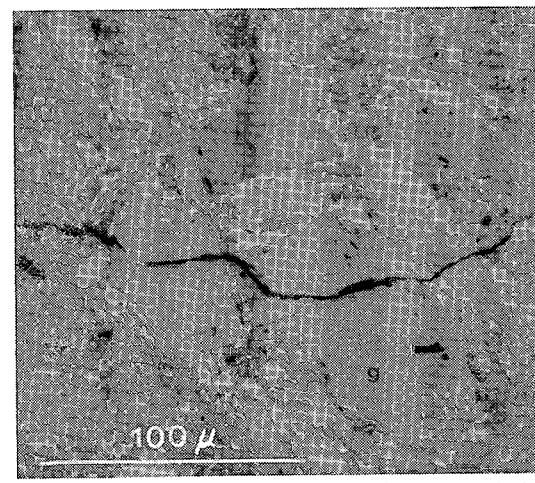

FIG. 5 Blocky grains of gustavite (flat grey, g) in a matrix of pyrrhotite (dark grey), bismuth and chalcopyrite (light shades of grey) partly penetrated by gustavite and other sulfosalts. Assemblage (6,3C) polished section, polarized light.

correlation is indicated between the Zn and Cd contents in the Tanco stannites (Fig. 4); a similar trend is suggested in stannites and kesterites from Mt. Pleasant, New Brunswick (Petruk 1973).

Černýite compositions are much closer to the end-member formula than the one from the Hugo permatite, South Dakota (Kissin *et al.* 1978), but kesterites from Tanco and Hugo are fairly similar. However, kesterite forms an abundant host to exsolved černýite in the Hugo pegmatite, whereas Tanco kesterite was identified only by a partial electron-microprobe analysis (Fig. 4) as a very thin zone within stannite of variable composition.

Gustavite (Harris & Chen 1975) occurs in angular to irregular grains up to 1 × 2 mm in size, associated with gladite–pekoite intergrowths, cosalite and other sulfosalts of the assemblage (6,3C). It penetrates the early granular pyrrhotite and native bismuth, replacing mainly the latter and forming extremely fine-grained emulsion-like structures with this phase (Fig. 5).

Six microprobe analyses of the Tanco gustavite are clustered close to the ideal composition $PbAgBi_3S_6$, except for substantial replacement of Bi by Sb (Table 6). Figure 6 shows a

TABLE 5. ELECTRON MICROPROBE ANALYSES OF STANNITE AND ČERNÝITE

	Stannite				Černýite		
Anal. #	S-8-1	S-8-2	S-8-4	S-8-6	S-8-II	S-8-III	S-8-IV
Cu	29.0	29.1	28.9	28.5	25.1	26.3	26.3
Fe	10.2	11.0	9.1	6.8	1.9	.7	.9
Zn	1.5	.8	3.6	4.7	1.8	1.6	1.3
Cd	2.4	2.4	3.7	4.1	17.9	19.2	19.3
Ag	n.d.*	n.d.	n.d.	n.d.	n.d.	.3	.3
Sn	27.1	26.1	26.7	26.7	25.1	24.8	24.6
Sb	.1	.8	.06	.06	-	-	-
S	30.0	29.8	29.9	29.0	27.3	26.5	26.4
	100.3	100.0	101.96	99.86	99.1	99.4	99.1

S-8-1 $Cu_{1.974}(Fe_{.792}Zn_{.100}Cd_{.091})_{\Sigma.983}(Sn_{.987}Sb_{.003})_{\Sigma.990}S_{4.053}$
S-8-2 $Cu_{1.987}(Fe_{.855}Cd_{.091}Zn_{.052})_{\Sigma.998}(Sn_{.954}Sb_{.030})_{\Sigma.984}S_{4.030}$
S-8-4 $Cu_{1.956}(Fe_{.701}Zn_{.236}Cd_{.160})_{\Sigma1.097}(Sn_{.967}Sb_{.002})_{\Sigma.969}S_{4.012}$
S-8-6 $Cu_{1.986}(Fe_{.540}Cd_{.159}Zn_{.318})_{\Sigma1.017}(Sn_{.995}Sb_{.004})_{\Sigma.999}S_{3.998}$
S-8-II $Cu_{1.883}(Cd_{.758}Fe_{.162}Zn_{.134})_{\Sigma1.054}Sn_{1.006}S_{4.057}$
S-8-III $(Cu_{1.995}Ag_{.014})_{\Sigma2.009}(Cd_{.824}Zn_{.116}Fe_{.063})_{\Sigma1.003}Sn_{1.007}S_{3.981}$
S-8-IV $(Cu_{2.001}Ag_{.014})_{\Sigma2.015}(Cd_{.831}Zn_{.097}Fe_{.077})_{\Sigma1.005}Sn_{1.001}S_{3.978}$

*not determined; Assemblage 6,3C
Analysts: S-8-II - D.C. Harris; others - D.R. Owens

TABLE 6. ELECTRON MICROPROBE ANALYSES OF GUSTAVITE

Assemblage	(6,3C)					
Anal.#	S-2	S-3	S-8-1	S-8-2	S-8A	S-16A
Ag	8.9	8.9	7.8	8.3	8.3	8.0
Pb	18.9	20.6	20.2	20.8	22.7	23.2
Bi	52.0	53.3	50.3	49.7	50.3	47.1
Sb	3.3	3.3	3.6	3.6	2.8	5.1
S	17.7	17.3	17.6	17.0	17.7	17.3
	100.8	103.4	99.5	99.4	101.8	100.7

		N	x	mol.%
S-2	$Ag_{.85}Pb_{.94}(Bi_{2.56}Sb_{.28})S_{5.69}$	3.64	.85	103.4
S-3	$Ag_{.83}Pb_{1.00}(Bi_{2.57}Sb_{.27})S_{5.43}$	3.65	.83	100.2
S-8-1	$Ag_{.72}Pb_{.98}(Bi_{2.42}Sb_{.30})S_{5.52}$	3.45	.73	101.0
S-8-2	$Ag_{.81}Pb_{1.06}(Bi_{2.51}Sb_{.31})S_{5.60}$	3.67	.81	96.7
S-8A	$Ag_{.82}Pb_{1.17}(Bi_{2.57}Sb_{.25})S_{5.89}$	3.82	.82	90.5
S-16A	$Ag_{.77}Pb_{1.16}(Bi_{2.33}Sb_{.43})S_{5.59}$	3.70	.77	90.6

Analyst: D.C. Harris.
Analyses S-2 and S-8-1 from Harris & Chen (1975).
N,x,mol.%($PbAgBi_3S_6$) - calculated from Pb/(Bi+Sb)/Ag ratios.
Crystallochemical formulas based on Σ Me=N+1.

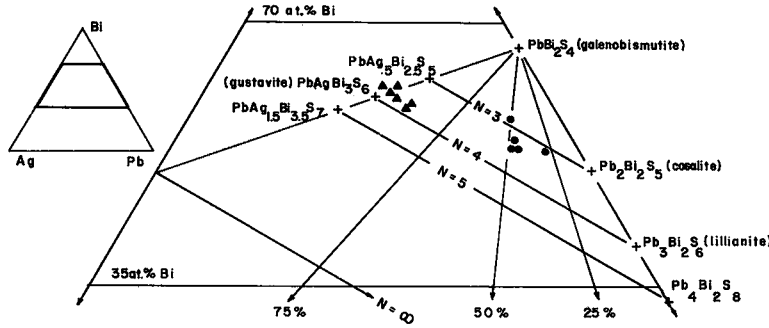

FIG. 6 Compositions of the Tanco gustavites (triangles) and cosalites (dots) in the Ag–Pb–Bi triangle (at.%). Values of *N* related only to the gustavite structure; the grid is modified after Makovicky & Karup-Møller (1977b). The values of Ag and Bi represent totals of Ag+Cu and Bi+Sb, respectively.

plot of these compositions in the system Ag–Pb–Bi, compared to coordinates devised for the crystallochemical relationships in the lillianite homologous series by Makovicky & Karup-Møller (1977a): *N*, average number of octahedra in diagonal chains running across individual "galena-like" layer motifs of the structure; *x*, the Ag + Bi⇌2Pb substitution coefficient, and the molecular percentage of the Ag–Bi end-member (*cf.*, Table 6).

In accordance with earlier results, summarized by Makovicky & Karup-Møller (1977b), *N* in the Tanco gustavites is somewhat lower than the ideal value of 4; compositions range between Gu_{90} and Gu_{103}. The only analyses that fall above the Gu_{100} limit, *S*-2 and *S*-8-1, do not yield mutually balanced coefficients and probably reflect analytical inaccuracies.

Cosalite was identified by X-ray powder diffraction of mineral mixtures from assemblage (6,3C), and by the electron microprobe. Five analyses recalculated on the basis of S=5 per quarter unit-cell (Table 7) indicate substitution of Ag and Cu for Pb (up to 16 at.% of the Pb, Ag, Cu total) and of Sb for Bi (up to 13 at.% of their total). Similar deviations from the ideal composition $Pb_2Bi_2S_5$ are evident in other modern analyses (*e.g.*, Povilaitis *et al.* 1969, Harada *et al.* 1972, Karup-Møller 1973, 1977; Nedachi *et al.* 1973, Srikrishnan & Nowacki 1974). This compositional complexity, as well as experimental evidence, strongly suggests that cosalite does not belong to the simple system Pb–Bi–S.

The structure of cosalite is closely related but does not belong to the true lillianite homologues as defined by Makovicky (1977) and Makovicky & Karup-Møller (1977a,b). One of the major

TABLE 7. ELECTRON MICROPROBE ANALYSES OF COSALITE, GLADITE, AND PEKOITE

Assemblage	Cosalite					Gladite	Pekoite	
	(6,3C)							
Anal.#	S-1	S-8-1	S-8-2	S-8A	S-8B	S-4*	S-4-1**	S-16
Cu	.2	.1	.2	1.1	.1	4.1	.6	.9
Pb	35.0	34.1	35.4	32.8	37.1	13.7	1.1	4.1
Bi	41.1	42.2	41.5	46.4	41.9	60.1	75.0	73.2
Sb	3.7	2.9	2.7	2.9	2.2	2.6***	3.5	4.1
Ag	3.2	3.2	2.8	.8	2.7	n.d.	n.d.	n.d.
S	17.3	16.9	16.5	18.0	17.0	18.3	19.0	19.2
	100.5	99.4	99.1	102.0	101.0	98.8	99.2	101.5

S-1 $(Pb_{1.571}Ag_{.278}Cu_{.028}) \Sigma 2.119 (Bi_{1.822}Sb_{.278}) \Sigma 2.100 S_{5.000}$

S-8-1 $(Pb_{1.565}Ag_{.284}Cu_{.019}) \Sigma 1.868 (Bi_{1.916}Sb_{.228}) \Sigma 2.144 S_{5.000}$

S-8-2 $(Pb_{1.661}Ag_{.252}Cu_{.029}) \Sigma 1.942 (Bi_{1.933}Sb_{.214}) \Sigma 2.147 S_{5.000}$

S-8A $(Pb_{1.409}Ag_{.062}Cu_{.152}) \Sigma 1.623 (Bi_{1.979}Sb_{.214}) \Sigma 2.193 S_{5.000}$

S-8B $(Pb_{1.689}Ag_{.236}Cu_{.019}) \Sigma 1.944 (Bi_{1.887}Sb_{.170}) \Sigma 2.057 S_{5.000}$

S-4* $Cu_{.970}Pb_{1.000}(Bi_{4.363}Sb_{.318})S_{8.636}$

S-4-1** $Cu_{.255}Pb_{.142}(Bi_{10.177}Sb_{.822})S_{16.800}$

S-16 $Cu_{.401}Pb_{.573}(Bi_{10.026}Sb_{.974})S_{17.159}$

Analyst: D.C. Harris.
Analyses S-4 and S-4-1 from Harris & Chen (1976).

*blebs and **host in a single exsolution intergrowth.
***not determined.

differences is the presence of Cu, randomly distributed in tetrahedral sites interstitial to the $Pb_2Bi_2S_5$ framework. Nevertheless, the formal stoichiometry of the Ag-rich and mostly Cu-poor Tanco cosalite can be examined within the same system Ag(+Cu)–Pb–Bi as was done for gustavite. Assuming a simple substitution (Ag, Cu)+Bi$\rightleftharpoons$2Pb, formulas derived from microprobe analyses and from the factors N and x match well in 4 out of 5 cases. Figure 6 shows the N values covering a wide range, mostly above the ideal value of 3. It also illustrates the high level of the [Ag(+Cu),Bi] substitution between 30 and 50 mol.% of the theoretical "end-member" composition $PbAg_{0.5}Bi_{2.5}S_5$.

The above treatment of cosalite is just another attempt to describe its crystal chemistry, which remains essentially unresolved. For example, Karup-Møller (1977) suggested [Pb,2(Ag, Cu)] substitution, possibly combined with [3Pb,2Bi+□], assuming fixed S=20 per unit cell. However, the Tanco cosalites do not follow the well-defined alignment of his samples in the (Ag+Cu) *vs.* Pb plot (Karup-Møller 1977, Fig. 8B).

Gladite–pekoite intergrowths occur in assemblage (6,3C). They form exsolution textures at the expense of an apparently homogeneous precursor (Fig. 7). This original phase was coarse-grained, as individual columnar crystals up to 1 × 4 cm can be recognized in hand specimens by their cleavage. Despite its crystallization as coarse subparallel aggregates, the homogeneous mineral was evidently a late phase which mainly replaced fine-grained masses of native bismuth, galena, chalcopyrite and pyrrhotite.

Microprobe analyses of the pekoite host and gladite blebs (Harris & Chen 1976) are listed in Table 7 together with another pekoite analysis. The position of the analyzed phases in the system PbS–Cu_2S–Bi_2S_3 in relation to ideal gladite $CuPbBi_5S_9$ and pekoite $CuPbBi_{11}S_{18}$ is illustrated in Figure 8. Estimated modes of the Tanco intergrowths indicate that pekoite/gladite ranges between about 8:1 and 5:1. Consequently, the bulk composition of the intergrowth contains about 90 mol.% Bi_2S_3.

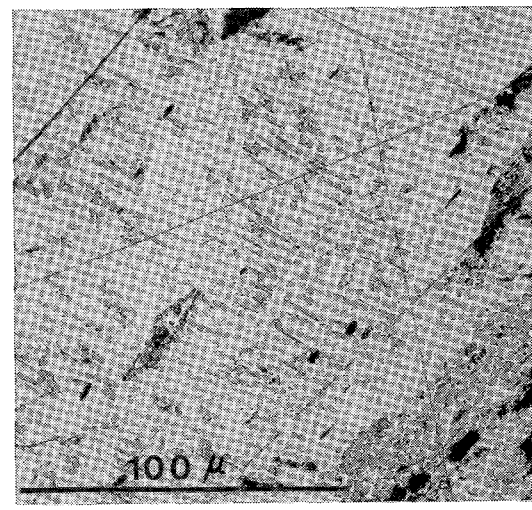

FIG. 7 Gladite exsolutions in pekoite matrix; the two sizes and orientations of the gladite blebs possibly indicate two generations. Assemblage (6,3C), polished section in oil immersion, etched with (1:1) HNO_3.

Tetrahedrite $(Cu>Ag)_{10}(Cu^*,Fe,Zn)_2Sb_3S_{13}$ and *freibergite* $(Ag>Cu)_{10}(Cu^*,Fe,Zn)_2Sb_3S_{13}$ are among the more common sulfosalts at Tanco, but their occurrence is erratic. Although aggregates up to 8 mm in size are found occasionally, most are just microscopic rims on chalcopyrite against pyrrhotite, bismuth and sphalerite.

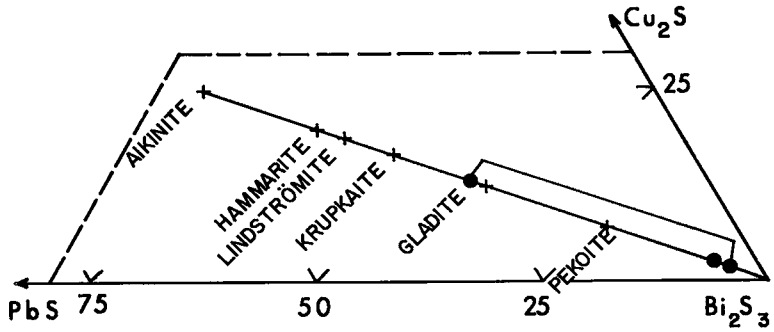

FIG. 8 Composition of the Tanco gladite and pekoite (dots) in the system PbS–Cu_2S–Bi_2S_3 (mol %), compared with the stoichiometric members of the aikinite–bismuthinite series (crosses).

TABLE 8. ELECTRON MICROPROBE ANALYSES OF FREIBERGITE, TETRAHEDRITE, AND MISCELLANEOUS SULFOSALTS

Assemblage	Freibergite		Tetrahedrite (6,3C)		Bournonite	Pyrargyrite	Miargyrite
Anal.#	S-1	S-3	S-8	S-16A	S-16A	S-1	S-I
Ag	29.6	32.0	19.1	10.8	n.d.	59.4	35.8
Cu	15.9	14.3	23.9	30.1	13.3	n.d.	n.d.
Pb	n.d.*	n.d.	n.d.	n.d.	42.5	n.d.	n.d.
Fe	5.3	6.0	.1	-	n.d.	n.d.	n.d.
Zn	-**	.5	6.4	5.6	n.d.	n.d.	n.d.
Bi	n.d.	.7	n.d.	n.d.	n.d.	n.d.	n.d.
Sb	26.6	26.7	25.6	27.2	23.3	23.6	41.7
As	-	.1	.5	-	n.d.	n.d.	n.d.
S	21.7	20.7	22.9	22.5	19.6	17.7	21.8
	99.1	101.0	98.5	96.2	98.7	100.7	99.3

S-1 $(Ag_{5.315}Cu_{4.685})_{\Sigma 10.000}(Cu_{.162}Fe_{1.838})_{\Sigma 2.00}Sb_{4.232}S_{13.110}$

S-3 $(Ag_{5.591}Cu_{4.242}Fe_{.169})_{\Sigma 10.002}(Fe_{1.858}Zn_{.143})_{\Sigma 2.001}(Sb_{4.117}Bi_{.062}As_{.024})_{\Sigma 4.221}S_{12.166}$

S-8 $(Cu_{6.746}Ag_{3.255})_{\Sigma 10.001}(Cu_{.167}Fe_{.033}Zn_{1.799})_{\Sigma 1.999}(Sb_{3.866}As_{.123})_{\Sigma 3.988}S_{13.127}$

S-16A $(Cu_{8.179}Ag_{1.821})_{\Sigma 10.000}(Cu_{.441}Zn_{1.559})_{\Sigma 1.999}Sb_{4.064}S_{12.766}$

S-16A $Cu_{1.036}Pb_{1.015}Sb_{.947}S_{3.026}$ S-1 $Ag_{2.973}Sb_{1.046}S_{2.980}$ S-I $Ag_{.980}Sb_{1.012}S_{2.008}$

Analysts: S-3 - T.T. Chen; others - D.C. Harris; *not determined; **not detected.

Four microprobe analyses indicate extreme variations in terms of $(Cu,Ag)_{10}$ and $(Cu^*,Fe,Zn)_2$ substitutions (Table 8). The two Ag-rich tetrahedrites with very low Fe contents seem to be exceptional among natural members of the series (Springer 1969, Petruk *et al.* 1971b, Shimada & Hirowatari 1972, Riley 1974, Charlat & Levy 1974), although natural and synthetic Ag-rich Zn_2-phases are known (Hall 1972).

The compositional variability of the Tanco tetrahedrites and freibergites may reflect, in part, their secondary metasomatic character indicated by textural relationships. Most of the Cu, Fe and Zn contents could have been inherited from the digested matrix, consisting of variable proportions of pyrrhotite, sphalerite and chalcopyrite.

Bournonite was found only in specimen *S*-16, closely associated with tetrahedrite, in a complex intergrowth with 9 other species. Despite the complex bulk chemistry of this aggregate, the bournonite corresponds, within the limits of analytical error, to the ideal formula $CuPbSbS_2$ (Table 8).

Pyrargyrite and *miargyrite* were identified in samples *S*-1, *S*-11 and *S*-16 as separate tiny inclusions in fine-grained aggregates of 10 to 12 species. Identification of both minerals is based on their nearly ideal stoichiometric compositions (Table 8) and optical properties; X-ray diffraction data could not be collected.

Paragenetic Relationships

Monomineralic occurrences of sphalerite (4,5A), molybdenite (4,5B), and sphalerite (6,3B) indicate only that most of Zn(+Cd) and almost all Mo migrated and precipitated separately from other sulfide components. Assemblage (6,3A), arsenopyrite + pyrrhotite + chalcopyrite in altered contacts of amphibolite xenoliths, is equally sterile in genetic information. Primary monoclinic pyrrhotite indicates temperatures below ~ 265°C at 2.5 kbar (Scott & Kissin 1973; S. A. Kissin, priv. comm. 1978) but the As contents of arsenopyrite suggest a temperature range 350–500°C (Kretschmar & Scott 1976, Fig. 7). The arsenopyrite–pyrrhotite geothermometer developed by these authors is not applicable, as the two minerals occur separately in two different reaction bands, and their stabilities are mutually exclusive.

High sulfidation state of Fe, fine-grained botryoidal aggregation and high Tl contents of pyrite and marcasite (6,3D) in open vugs with calcite and cookeite indicate a late low-temperature origin, at a $f(S_2)$ possibly higher than in any other sulfide assemblage of the pegmatite.

The complex assemblages (4,5C) and (6,3C) are the only ones that provide several clues to their mode of crystallization.

Assemblage (4,5C)

This assemblage consists of antimonian bismuth, bismuthian antimony, arsenic and galena with very subordinate sphalerite, chalcopyrite, tetrahedrite and dyscrasite (Table 2). Trace quantities of unidentified sulfosalts have also been detected. In terms of decreasing elemental abundances, the assemblage consists mainly of Bi,Pb,S,As,Sb and minor Zn(Cd),Cu and Ag.

The mineralogical phase rule is violated in the assemblage as a whole ($P \geqslant 11$, $C=8$), and also in the mineral associations of individual sulfide patches. However, it is difficult to identify specific departures from equilibrium because of the

presence of complex phases like argentian tetrahedrite and the unidentified sulfosalts.

Both native arsenic and antimony occur in contact with stibarsen, but separately. Their textural features suggest partly successive, partly simultaneous crystallization. Exsolution intergrowths typical of AsSb–Sb and AsSb–As pairs from other localities (Quensel *et al.* 1937, Wretblad 1941, Černý & Harris 1973) or other reaction phenomena were not observed. Disequilibrium is strongly indicated here, despite the poor understanding of the subsolidus relations in the system As–Sb (Skinner 1965, Leonard *et al.* 1971, Clark 1972) and a possible influence of Bi concentration.

The fine-grained guttate intergrowths of bismuth and galena which surround most of the coarser-grained aggregates suggest quench-induced mass precipitation in the last stages of crystallization (Fig. 1). An exsolution origin is unlikely as no possible precursors are known along the Bi–PbS join (Craig 1967).

Assuming that the effect of pressure on thermal stabilities of most native elements, alloys, sulfosalts and sulfides is negligible (Craig 1967, Barton 1970, Kretschmar & Scott 1976), crystallization of assemblage (4,5C) may be placed below approx. 270°C, the melting point of Bi. Slight rise of this melting temperature with increasing Sb content (Hansen & Anderko 1958) is more than sufficiently counterbalanced by the negative effect of increasing pressure (Klement *et al.* 1963). The primary, non-exsolved nature of the Sb, As and AsSb aggregates suggests crystallization temperatures well below the field of continuous solid solution at 300°C (Skinner 1965), possibly as low as 250–185°C (Clark 1972).

Assemblage (6,3C)

This assemblage consists of at least 21 mineral species (Table 1). The number of elemental components is, as in the preceding case, much lower: Bi, S, Pb and Sb are most abundant, Cu, Fe and Ag are subordinate; minor Zn, Cd, Sn and As are the only other significant components. Similar predominance of phases over components is also typical of individual sulfide aggregates that contain as many as 13 species.

Table 9 shows the bulk chemistry and mineral composition of four such aggregates selected for their diversified mineral content. Variations in subordinate components have profound influence on the mineral assemblages: *e.g.*, Zn and Cd abundances control the appearance of sphalerite or hawleyite, and Ag contents regulate the crystallization of gustavite, cosalite, tetrahedrite or freibergite. On the other hand, appearance of miargyrite in the Ag-poor assemblage *S*-16 and the presence of kesterite and černýite in the Zn, Cd-poor sample *S*-8 suggest local reactions and equilibria in a bulk aggregate that is not equilibrated as a whole.

TABLE 9. BULK COMPOSITION OF SULFIDE AGGREGATES

Sample #	S-2	S-3	S-8	S-16
Bi	63.00	66.50	75.00	75.62
Sb	2.88	2.78	2.62	2.82
Pb	6.62	7.92	3.00	3.12
Cu	1.88	2.86	1.09	.98
Ag	.90	1.53	.068	.064
Fe	12.00	7.55	.88	1.18
Mn	.004	.009	.008	.07
Zn	.062	.28	.014	.031
Cd	.36	.76	.004	.015
S	11.69	9.27	15.80	16.11
	99.396	99.459	98.484	100.01
BISMUTH	X	X	X	X
SPHALERITE	+	+		+
HAWLEYITE	+	+		
PYRRHOTITE	X	X	+	+
ARSENOPYRITE		+	+	
CHALCOPYRITE	+	+	+	+
GALENA		+		
CUBANITE	+			
STANNITE			+	+
ČERNÝITE			+	
KESTERITE			+	
GUSTAVITE	X	X	+	+
COSALITE			+	
GLADITE-PEKOITE			X	X
TETRAHEDRITE	+		+	+
FREIBERGITE		+		
BOURNONITE				+
PYRARGYRITE		+		
MIARGYRITE				+
(CASSITERITE			+	+)

X - substantial component
\+ - subordinate to trace amount

From textural relationships, a general two-stage sequence of crystallization can be inferred (Table 10): (1) The first minerals to crystallize

TABLE 10. PROBABLE EVOLUTION OF THE SULFIDE MINERAL ASSEMBLAGE (6,3C)

PRE-EXISTING PHASES	EARLY ASSOCIATION	LATE ASSOCIATION
Sn	Fe,Cu,Bi,Zn,Cd,(As)	Pb,Ag,Sb
CASSITERITE ← STANNITE	PYRRHOTITE	GLADITE-PEKOITE
← KESTERITE	CHALCOPYRITE	GUSTAVITE
← ČERNÝITE	SPHALERITE	COSALITE
	HAWLEYITE	TETRAHEDRITE--FREIBERGITE
	BISMUTH	GALENA
	CUBANITE	BOURNONITE
	(GALENA?)	PYRARGYRITE
		MIARGYRITE
		ANTIMONY

were the sulfides of Fe, Cu, Zn and Cd: pyrrhotite, chalcopyrite, cubanite, arsenopyrite, sphalerite and hawleyite, closely followed by bismuth and some galena. They were mostly deposited on the enclosing silicates, forming a lining between these and later sulfosalts. Cassiterite is the only preexisting phase corroded and replaced by these early sulfides (Fig. 2,3). Minerals of the stannite group evidently derived their Sn content from cassiterite, and the different species were generated according to local and temporal fluctuations in the activities of Fe, Zn and Cd. (2) The second mineral sequence consists of galena and a variety of sulfosalts accumulated mainly in the central parts of sulfide aggregates, and crystallized at least in part at the expense of the early suite. These later phases represent a substantial addition of Pb, Ag and Sb to the Bi, Fe, Cu, Zn, Cd and Sn of the earlier minerals. Replacements, such as tetrahedrite corrosion of chalcopyrite and pyrrhotite, gladite–pekoite after chalcopyrite and bismuth, and gustavite replacing bismuth amply demonstrate the metasomatic character of the second mineral suite (Figs. 5,9).

Exceptions to the above generalization can be observed on small scale. Chalcopyrite occasionally appears among the youngest minerals of the late mineral sequence, as veins and linings of microscopic vugs in sulfosalts. Tetrahedrite seems to coexist with chalcopyrite in some specimens. Nevertheless, the exceptions seem to be quantitatively insignificant compared with the main course of events shown in Table 10.

The variety of sulfosalts is mainly responsible for the excess of phases over components. Non-

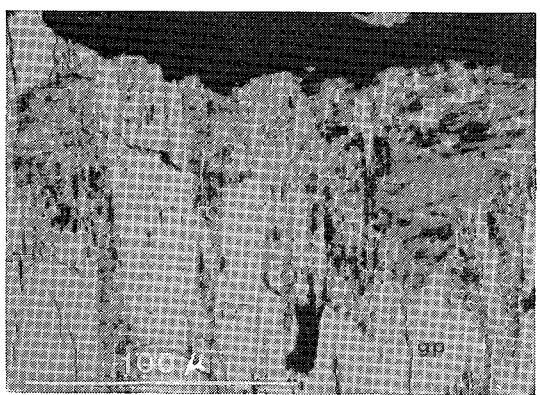

FIG. 9 Subparallel blades of the gladite–pekoite precursor (mottled light grey, gp) cross-cutting subhorizontally banded fine-grained bismuth, pyrrhotite and chalcopyrite. Assemblage (6,3C), polished section in oil immersion, crossed polars.

equilibrium assemblages are typical of this mineral subclass which suffers from the "plague of small ΔG's" (Craig & Barton 1973; *cf.*, Shcherbina 1967). Disequilibrium is also indicated by the wide variety of replacement textures and by the different stages at which incomplete reactions were interrupted. Extremely fine-grained patches in these aggregates of reactants and products strongly suggest quenching as the main factor responsible for arresting the replacement reactions.

Non-equilibirum is also suggested by the occurrence of hawleyite, considered metastable under all conditions (Craig & Scott 1974). Within the ranges of $f(S_2)$ and T derived below, sphalerite should also be metastable and wurtzite should have formed instead (Scott & Barnes 1972). However, the influence of substantial (Zn,Cd) diadochy (Table 3) on the polymorphism at low temperatures is not yet known (Kröger 1940, Charbonnier & Murat 1974). The effect of sulfur or metal deficiency on the greenockite–hawleyite stabilization is also unexplored (Clark & Sillitoe 1971, Oen *et al.* 1974).

Crystallization temperature of assemblage (6,3C) is limited by the melting of Bi at about 270°C and by the upper stability limit of primary monoclinic pyrrhotite at approximately 265°C at 2.5 kbar (Scott & Kissin 1973, S.A. Kissin, priv. comm. 1978). Sphalerite compositions (10–12 mol.% FeS), possibly in equilibrium with pyrrhotite, may indicate temperatures much lower than these maximum values, *i.e.*, between 200-150° (Scott & Kissin 1973). Untwinned orthorhombic cubanite associated with pyrrhotite also suggests temperatures below 200–210°C for the onset of crystallization (Cabri *et al.* 1973), whereas pyrargyrite is stable above 192°C (Chang 1963, Hall 1966). The lack of exsolution textures in stannite-group minerals indicates simultaneous or sequential crystallization (Fig. 3). Compared with the experimental results of Springer (1972) and Harris & Owens (1972), the Zn–Fe partitioning in the Tanco stannite and kesterite (Fig. 4) suggests temperatures well below 200°C (*cf.*, Petruk 1973). However, the experiments were performed on essentially Cd-free phases, whereas the Tanco minerals are considerably enriched in this element (Table 5).

Minerals of the assemblage (6,3C) and their thermal limits indicate low values of $f(S_2)$ during crystallization, distinctly below Barton's (1970) "main line" of ore-forming environments (Fig. 10). In the absence of bismuthinite and pyrite, the reactions Bi–bismuthinite and pyrrhotite–pyrite represent the upper T, $f(S_2)$ limit; arsenopyrite found in a single specimen asso-

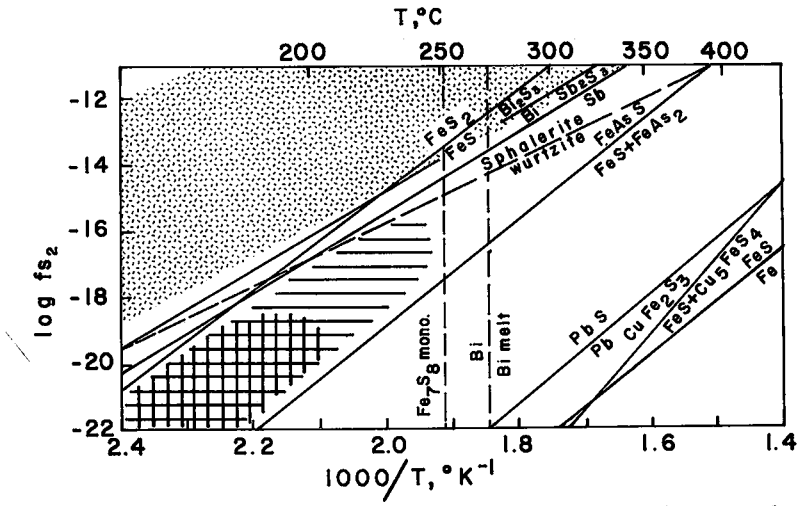

FIG. 10 Sulfidation reactions and stability boundaries pertinent to the crystallization of assemblage (6,3C). Compiled and partly extrapolated from Barton (1970), Craig & Barton (1973), Craig & Scott (1974), Kretschmar & Scott (1976), Scott & Barnes (1972), and Scott & Kissin (1973). The stippled area shows the "main line" ore-forming environment of Barton (1970). The ruled area is the possible field, and the cross-hatched area is the probable field of crystallization of assemblage (6,3C).

ciated with pyrrhotite may possibly indicate the pyrrhotite + löllingite–arsenopyrite reaction as the lower boundary. Thus, $f(S_2)$ could not surpass 10^{-16} atm, and probably was as low as 10^{-20} to 10^{-22} atm.

SUMMARY

Sulfide minerals belong to the latest assemblages crystallized in the two innermost zones of the Tanco pegmatite. The spodumene-(petalite-) rich zones (4) and (5) carry disseminated sphalerite and molybdenite, and patches of Bi, Pb,As,Sb minerals with minor Zn(Cd), Cu and Ag. The central microcline + quartz zone (6), modified by Ta,Nb,Be,Sn,Zr(Hf)-bearing albitization (3), contains an Fe,Cu,As-assemblage in contacts with amphibolite xenoliths, Tl-enriched Fe disulfides in open vugs, and disseminated sphalerite. The main sulfide content of this zone consists of a cavity- and fracture-filling assemblage with an early Fe,Cu,Zn,Cd,Sn, Bi (and Pb) association of simple sulfides, followed and partly replaced by an array of sulfosalts containing, in addition, substantial Pb, Ag, and Sb. In both parent zones, the complex assemblages are not equilibrated; they show indications of quenching in the last stages of crystallization and replacement processes. The precipitation started distinctly below 270–250°C, probably about 200°C, and it could have proceeded to about 150°C. Fugacity of S_2 could not surpass 10^{-16} atm, and was probably as low as 10^{-20} to 10^{-22} atm.

Sulfide phases containing As, Bi, Fe, Cu, Zn and Mo are relatively common in granitic pegmatites, although only in trace quantities. In contrast, sulfide minerals with substantial Sb, Pb, Ag, Cd and Sn are only rarely found; they tend to be restricted to those pegmatite types that show considerable enrichment in Li, Rb, Cs, Ta, B, and F. The Varuträsk deposit in Sweden (Ödman 1942, Quensel *et al.* 1937, Quensel 1956), the Viitaniemi pegmatite in Finland (Volborth 1960), and the Mangualde pegmatite in Portugal (Oen 1959, 1970; Oen *et al.* 1973, Oen & Kieft 1976) may serve as examples of this type. Sulfide mineralization closely similar to that of the Tanco pegmatite is currently being studied in the Hugo, Tip Mountain, and other lithium-rich pegmatites of the Black Hills, South Dakota (Kissin *et al.* 1978; W.L. Roberts, pers. comm. 1977). It is noteworthy in this respect that the Tanco and related pegmatites in southeastern Manitoba seem to have the same petrogenetic history as the pegmatites of the southern Black Hills (Černý & Trueman 1978).

ACKNOWLEDGEMENTS

The authors are indebted to Messrs. C.T. Williams, J.C. Heyward, R. A. Crouse and G. Hecke of the Tantalum Mining Corporation of Canada who supported field work and helped in collecting sulfide specimens. Part of the microprobe work was carried out by D.R. Owens, T.T. Chen and J.H.G. Laflamme (CANMET), and the bulk compositions of four sulfide aggregates were analyzed by R. Gordon (University of Copenhagen) and J.T. Szymański and J.D. Grice, and several students of the first author (University of Manitoba) assisted with the X-ray diffraction studies. Drs. S.A. Kissin (Lakehead University), E. Makovicky (University of Copenhagen) and J.T. Szymański (CANMET) made some of their manuscripts available prior to publication and offered helpful suggestions. The study was supported by the National Research Council of Canada grant A–7948 to the first author.

REFERENCES

ANGELELLI, V., ROSALES, A. & SCHALAMUK, I.B. (1971): Geoquimica del renio. Un esayo en molibdenitas argentinas. *Rev. Assoc. Geol. Argent.* **26**, 153-161.

AYRES, D. (1974): Distribution and occurrence of some naturally-occurring polytypes of molybdenite in Australia and Papua New Guinea. *J. Geol. Soc. Aust.* **21**, 273-278.

BARTON, P.B., JR. (1970): Sulfide petrology. *Mineral. Soc. Amer. Spec. Pap.* **3**, 187-198.

BOYLE, R.W. (1969): Conditions for the formation of rhombohedric (3*R*) molybdenite. *Sov. Phys. Dokl.* **13**, 1089-1090.

CABRI, L.J., HALL, S.R., SZYMAŃSKI, J.T. & STEWART, J. M. (1973): On the transformation of cubanite. *Can. Mineral.* **12**, 33-38.

ČERNÝ, P. & HARRIS, D.C. (1973): Allemontite and its alteration products from the Odd West pegmatite, southeastern Manitoba. *Can. Mineral.* **11**, 978-984.

——— & SIMPSON, F.M. (1978): The Tanco pegmatite at Bernic Lake, Manitoba. X. Pollucite. *Can. Mineral.* **16**, 325-333.

——— & TRUEMAN, D.L. (1978): Distribution and petrogenesis of lithium pegmatites in the western Superior province of the Canadian Shield. *Energy* (in press).

CHANG, L.L.Y. (1963): Dimorphic relation in Ag_3SbS_3. *Amer. Mineral.* **48**, 429-432.

CHARBONNIER, M. & MURAT, M. (1974): Sur la détermination des diagrammes de phases à température ambiante des sulfures mixtes appartenant aux systèmes Zn–Cd–S, Zn–Hg–S, Cd–Hg–S. *C.R. Acad. Sci. Paris* **278** (C), 259-261.

CHARLAT, M. & LEVY, C. (1974): Substitutions multiples dans la série tennantite–tetraédrite. *Soc. franç. Minéral. Crist.* **97**, 241-250.

CLARK, A.H. (1970): Compositional differences between hexagonal and rhombohedral molybdenite. *Neues Jahrb. Mineral. Monatsh.* 33-38.

——— (1971): Molybdenite $2H_1$, molybdenite 3*R*, and jordisite from Carrizal Alto, Atacama, Chile. *Amer. Mineral.* **56**, 1832-1835.

——— (1972): Mineralogy of the Alacrán deposit, Pampa Larga, Chile. VI. Antimonian arsenic alloys. *Neues Jahrb. Mineral. Monatsh.*, 447-454.

——— & SILLITOE, R.H. (1971): Hawleyite from Mina Coquimbana (Cerro Blanco), Atacama Province, Chile. *Neues Jahrb. Mineral. Monatsh.*, 205-210.

CRAIG, J.R. (1967): Phase relations and mineral assemblages in the Ag–Bi–Pb–S system. *Mineral. Deposita* **1**, 278-306.

——— & BARTON, P.B., JR. (1973): Thermochemical approximations for sulfosalts. *Econ. Geol.* **68**, 493-506.

——— & SCOTT, S.D. (1974): Sulfide phase equilibria. *Mineral. Soc. Amer. Short Course Notes* **1**, CS1-110.

CROUSE, R.A. & ČERNÝ, P. (1972): The Tanco pegmatite at Bernic Lake, Manitoba. I. Geology and paragenesis. *Can. Mineral.* 11, 591-608.

FRONDEL, J.W. & WICKMAN, F.E. (1970): Molybdenite polytypes in theory and occurrence. II. Some naturally-occurring polytypes of molybdenite. *Amer. Mineral.* **55**, 1857-1875.

HALL, A.J. (1972): Substitution of Cu by Zn, Fe, and Ag in synthetic tetrahedrite, $Cu_{12}Sb_4S_{13}$. *Soc. franç. Minéral. Crist. Bull.* **95**, 583-594.

HALL, H.T. (1966): *The Systems Ag–Sb–S, Ag–As–S, and Ag–Bi–S: Phase Relations and Mineralogical Significance.* Ph.D. thesis. Brown Univ., Providence, R.I.

HANSEN, M. & ANDERKO, K. (1958): *Constitution of Binary Alloys.* McGraw-Hill, New York.

HARADA, K., HAGASHIMA, K. MIYOKAWA, K. & YUI, S. (1972): Bismuthinite and cosalite from Agenosawa mine, Akita Prefecture, Japan. *J. Geol. Soc. Japan* 78, 485-488.

HARRIS, D.C. & CHEN, T.T. (1975): Gustavite: two Canadian occurrences. *Can. Mineral.* **13**, 411-414.

——— & ——— (1976): Crystal chemistry and re-examination of nomenclature of sulfosalts in the aikinite–bismuthinite series. *Can. Mineral.* **14**, 194-205.

——— & OWENS, D.R. (1972): A stannite–kesterite exsolution from British Columbia. *Can. Mineral.* **11**, 531-534.

KARUP-MØLLER, S. (1973): A gustavite–cosalite–galena–bearing mineral suite from the cryolite deposit at Ivigtut, South Greenland. *Medd. Grønland* **195** (5), 1-40.

——— (1977): Mineralogy of some Ag–(Cu)–Pb–Bi sulphide associations. *Geol. Soc. Denmark Bull.* **26**, 41-68.

KEIGHIN, C.W. & HONEA, R.M. (1969): The system Ag–Sb–S from 600°C to 200°C. *Mineral. Deposita* **4**, 153-171.

KHURSHUDYAN, E.Kh. (1967): Mode of origin of the rhombohedral modification of molybdenite. *Dokl. Acad. Sci. U.S.S.R. (Earth Sci. Sect.)* **171**, 149-151.

KISSIN, S.A. (1974): *Phase Relations in a Portion of the Fe–S System.* Ph. D. thesis, Univ. Toronto.

———, OWENS, D.R. & ROBERTS, W.L. (1978): Černýite, a copper–cadmium–tin sulfide with the stannite structure. *Can. Mineral.* **16**, 139-146.

KLEMENT, W., JR., JAYARAMAN, A. & KENNEDY, G.C. (1963): Phase diagrams of arsenic, antimony, and bismuth at pressures up to 70 kbars. *Phys. Rev.* **131**, 632-637.

KRETSCHMAR, U. & SCOTT, S.D. (1976): Phase relations involving arsenopyrite in the system Fe–As–S and their application. *Can. Mineral.* **14**, 364-386.

KRÖGER, F.A. (1940): Solid solutions in the ternary system ZnS–CdS–MnS. *Z. Krist.* **102**, 132-135.

LEONARD, B.F. MEAD, C.W. & FINNEY, J.J. (1971): Paradocrasite, $Sb_2(Sb,As)_2$, a new mineral. *Amer. Mineral.* **56**, 1127-1146.

MAKOVICKY, E. (1977): Chemistry and crystallography of the lillianite homologous series. III. Crystal chemistry of lillianite homologues. Related phases. *Neues Jahrb. Mineral. Abh.* **131**, 187-207.

——— & KARUP-MØLLER, S. (1977a): Chemistry and crystallography of the lillianite homologous series. I. General properties and definitions. *Neues Jahrb. Mineral. Abh.* **130**, 264-287.

——— & ——— (1977b): Chemistry and crystallography of the lillianite homologous series. II. Definition of new minerals: eskimoite, vikingite, ourayite and treasurite. Redefinition of schirmerite and new data on the lillianite–gustavite solid-solution series. *Neues Jahrb. Mineral. Abh.* **131**, 56-82.

NEDACHI, M., TAKEUCHI, T., YAMAOKA, K. & TANIGUCHI, M. (1973): Bi–Ag–Pb–S minerals from the Agenosawa Mine, Akita Prefecture, Northeastern Japan. *Sci. Rep. Tohoku Imp. Univ. (Ser. 3)* **12**, 69-80.

ÖDMAN, O.H. (1942): Minerals of the Varuträsk pegmatite. XXXII. Native metals and sulphides. *Geol. Foren. Förh.* **64**, 277-282.

OEN, I.S. (1959): On some sulphide minerals in the beryllium–lithium pegmatite of Mangualde, North Portugal. *Neues Jahrb. Mineral. Abh.* **93**, 192-208.

——— (1970): Paragenetic relations of some Cu–Fe–Sn sulfides in the Mangualde pegmatite, north Portugal. *Mineral. Deposita* **5**, 59-84.

———, BURKE, E.A.J. & KIEFT, C. (1973): Bismuthian tennantite from Mangualde, Portugal. *Neues Jahrb. Mineral. Monatsh.*, 43-46.

———, KAGER, P. & KIEFT, C. (1974): Hawleyite and greenockite in ores from Los Blancos, Sierra de Cartagena, Spain. *Neues Jahrb. Mineral. Monatsh.*, 507-513.

——— & KIEFT, C. (1976): Silver-bearing wittichenite–chalcopyrite–bornite intergrowths and associated minerals in the Mangualde pegmatite, Portugal. *Can. Mineral.* **14**, 185-193.

PETRUK, W. (1973): Tin sulphides from the deposit of Brunswick Tin Mines Limited. *Can. Mineral.* **12**, 46-54.

———, HARRIS, D.C., CABRI, L.J. & STEWART, J.M. (1971a): Characteristics of the silver–antimony minerals. *Can. Mineral.* **11**, 187-195.

——— & STAFF (1971b): Characteristics of the sulphides. *Can. Mineral.* **11**, 196-231.

POVILAITIS, M.M., MOZGOVA, N.N. & SENDEROVA, V.M. (1969): Bismuth minerals in the Dzhida molybdenum–tungsten deposit (western Transbaikalia) *Zap. Vses. Mineral. Obshchest.* **98**, 655-664 (In Russ.).

QUENSEL, P. (1956): The paragenesis of the Varuträsk pegmatite, including a review of its mineral assemblage. *Ark. Mineral. Geol.* **2**, 9-125.

———, AHLBORG, K. & WESTGREN, A. (1937): Minerals of the Varuträsk pegmatite. II. Allemontite, with an X-ray analysis of the mineral and of other arsenic-antimony alloys. *Geol. Fören. Förh.* **59**, 135-144.

RILEY, J.F. (1974): The tetrahedrite-freibergite series, with reference to the Mount Isa Pb–Zn–Ag orebody. *Mineral. Deposita* **9**, 117-124.

RUCKLIDGE, J. & GASPARRINI, E. (1969): Electron microprobe analytical data reduction, EMPADR VII. *Dep. Geology, Univ. Toronto.*

SCOTT, S.D. & BARNES, H.L. (1972): Sphalerite–wurtzite equilibria and stoichiometry. *Geochim. Cosmochim. Acta* **36**, 1275-1295.

——— & KISSIN, S.A. (1973): Sphalerite composition in the Zn–Fe–S system below 300°C. *Econ. Geol.* **68**, 475-479.

SHCHERBINA, V.V. (1967): Principles of combination of cations and anions during the formation of sulfosalts. *Geochem. Int.* **4**, 1104 (Abstr.).

SHIMADA, N. & HIROWATARI, F. (1972): Argentian tetrahedrites from the Taishu-Shigekuma mine, Tsushima Island, Japan. *Mineral J. (Japan)* **7**, 77-87.

SKINNER, B.J. (1961): Unit-cell edges of natural and synthetic sphalerites. *Amer. Mineral.* **46**, 1399-1411.

——— (1965): The system arsenic–antimony *Econ. Geol*, **60**, 228-239.

SOMANCHI, S. (1966): Subsolidus phase relations in the system Ag–Sb. *Can. J. Earth Sci.* **3**, 211-222.

SPRINGER, G. (1969): Electron probe analyses of tetrahedrite. *Neues Jahrb. Mineral. Monatsh.*, 24-32.

——— (1972): The pseudobinary system Cu_2FeSnS_4–Cu_2ZnSnS_4 and its mineralogical significance. *Can. Mineral.* **11**, 535-541.

SRIKRISHNAN, T. & NOWACKI, W. (1974): A redetermination of the crystal structure of cosalite, $Pb_2Bi_2S_5$. *Z. Krist.* **140**, 114-136.

SZYMAŃSKI, J.T. (1978): The crystal structure of černýite, Cu_2CdSnS_4, a cadmium analogue of stannite. *Can. Mineral.* **16**, 147-151.

VOLBORTH, A. (1960): Gediegen Wismutantimon und andere Erzmineralien im Li–Be–Pegmatit von Viitaniemi, Eräjärvi, Zentral Finnland. *Neues Jahrb. Mineral. Abh.* **94**, 140-149.

WRETBLAD, P.E. (1941): Minerals of the Varuträsk pegmatite. XX. Die Allemontite und das System As–Sb. *Geol. Fören. Förh.* **63**, 19-48.

YANG, MIN-CHIH, NI, CHI-TSUNG, TAI, FENG-FU & WANG, KUAN-HSIN (1975): Geological characteristics of molybdenum deposits from a certain district, China, with special reference to platinum metals in molybdenum ore minerals. *Ti Ch'iu Hua Hsueh* (*Geochim.*) 11-22 (in Chin.).

ZNAMENSKIY, V.S., LEBEDEV, L.M. & SIDORENKO, G.A. (1970): Molybdenite from volcanic rocks of Quaternary age on Iturup Island, Kurile Islands. *Dokl. Acad. Sci. U.S.S.R.* (*Earth Sci. Sect.*) **193**, 143-146.

Received May 1978; revised manuscript accepted July 1978.